Dynamic Response of the LE-5 Rocket Engine Liquid Oxygen Pump

T. Shimura* and K. Kamijo†
National Aerospace Laboratory of Japan, Miyagi, Japan

A three-stage H-1 rocket has been developed, the second stage of which has a LOX/LH_2 engine, LE-5. Regarding the POGO phenomenon of the second stage of the H-1 rocket, analyses are being conducted in order to determine whether or not a POGO suppression device is necessary for the LE-5 engine. In this study, the dynamic characteristics of the liquid oxygen pump of the LE-5 engine were examined by artificially creating periodical perturbations in the pump flow in order to obtain the data necessary for POGO analysis of the H-1 rocket.

Nomenclature

A_i = pump inlet cross-sectional area
C_b = cavitation compliance
f_{cr} = resonant frequency
g = gravitational acceleration
h = dimensionless head, $H/(u_t^2/g)$
H = head
ΔH = pump delivery head fluctuation, $\tilde{h}_2 - \tilde{h}_1$
j = imaginary index
L = inertance
M_b = mass flow gain factor
N = rotational speed
Q = flow rate, dimensionless for fluctuating quantity, $Q/(NQ_d/N_d)$
R = resistance
S = sucuon specific speed, $NQ^{0.5}/(NPSH)^{0.75}$
u_t = impeller tip velocity
V_c = cavity volume
Z_{ij} = pump transfer matrix component
μ = pump dynamic gain factor
ω = angular velocity

Superscripts

$\tilde{(\ )}$ = fluctuating quantity
$\bar{(\ )}$ = mean quantity
$(\ )^*$ = cavitation breakdown point value

Subscripts

1 = pump inlet
2 = pump outlet
d = design point
ij = component number
p = pump

Introduction

IT is common for turbopumps of rockets to be operated in low net positive suction head (NPSH) conditions. Therefore, oscillation of propellant feed systems associated with cavitation is often encountered. When this feedline oscillation mode is in tune with the structural mode of a rocket, provided there is sufficient engine gain and phase to produce instability, longitudinal vibration of the rocket referred to as "POGO" occurs.[1,2] Because the characteristics of turbopumps are closely related to POGO phenomena, studies of turbopump dynamic characteristics have been made.[3-11] However, because of experimental difficulties, particularly in measuring dynamic flow rate, general results are not available.

Brennen and Acosta[6] studied the dynamic characteristics of cavitating inducers analytically and tried to express their characteristics by a transfer matrix, Z, which consists of four components as shown in the following equation.

$$\begin{pmatrix} \tilde{h}_2 - \tilde{h}_1 \\ \tilde{Q}_2 - \tilde{Q}_1 \end{pmatrix} = \begin{bmatrix} Z_{11} & Z_{12} \\ Z_{21} & Z_{22} \end{bmatrix} \begin{pmatrix} \tilde{h}_1 \\ \tilde{Q}_2 \end{pmatrix} \tag{1}$$

Ng and Brennen et al.[7,8] conducted an ingenious experiment in order to examine the dynamic behavior of cavitating inducers and obtained the characteristics of the transfer matrix of a cavitating inducer. With regard to the dynamic characteristics of a centrifugal pump with an inducer, such as a liquid propellant feed pump, it might be reasonably assumed that the results of the cavitation compliance component, Z_{21}, and the mass flow gain factor component, Z_{22}, used in the analysis of the cavitating inducer, should be applicable to a centrifugal pump. However, the other two components, Z_{11} and Z_{12}, are expected to be considerably different from the results of the cavitating inducers, since the delivery head of cavitating inducers is strongly influenced by cavitation, while that of centrifugal pumps is not affected as much.

The present study was mainly conducted in order to obtain experimental data on the two components, Z_{11} and Z_{12}, of the transfer matrix of a centrifugal pump with an inducer. The pump was a liquid oxygen pump for the LE-5 rocket engine and was tested using liquid nitrogen. From relationship (1), the following equation is obtained.

$$\tilde{h}_2 - \tilde{h}_1 = Z_{11}\tilde{h}_1 + Z_{12}\tilde{Q}_1 \tag{2}$$

Substituting two independent sets of data, $\tilde{h}_{1i}$, $\tilde{h}_{2i}$ and $\tilde{Q}_{1i}$ $(i = 1,2)$, into Eq. (2), two equations for Z_{11} and Z_{12} are obtained. Then the Z_{11} and Z_{12} components are determined by solving these two equations simultaneously. The Z_{12} component values were determined by two different methods. One set of values was determined by simultaneously solving the two equations as mentioned above. Another was determined using one set of data assuming that the Z_{11} component was small and negligible, that is $\tilde{h}_2 - \tilde{h}_1 = Z_{12}\tilde{Q}_1$, under high NPSH conditions. Consequently, Z_{12} was determined by the equation $Z_{12} = (\tilde{h}_2 - \tilde{h}_1)/\tilde{Q}_1$. The effects of the pump rotating speed and pump mean flow rate on the Z_{12} component were also examined.

An ultrasonic flow meter[12] was used to measure the dynamic flow rate. A slit type perturbing valve was used to cause

Presented as Paper 83-1385 at the AIAA/SAE/ASME 19th Joint Propulsion Conference, Seattle, Wash., June 27-29, 1983; submitted July 26, 1983; revision received April 3, 1984. This paper is declared a work of the Japanese Government and therefore is in the public domain.

*Senior Researcher, Rocket Fluid Systems Section.
†Head, Rocket Fluid Systems Section. Member AIAA.

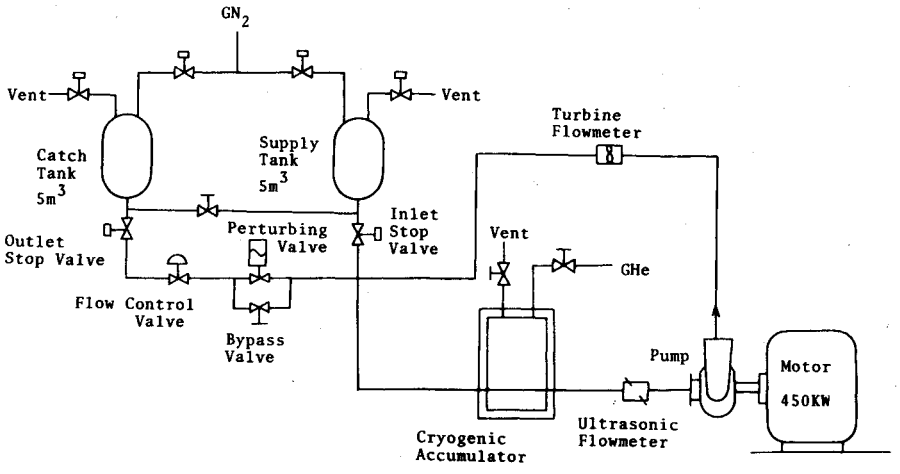

Fig. 1 Test facility.

periodical oscillations in the pump flow. Tests were conducted in the frequency range of 1 to 45 Hz. Independent sets of data having different phase relations were obtained by varying the helium gas volume in a vacuum-jacketed cryogenic accumulator which was installed in the pump inlet line. Amplitude and phase of all experimental data were determined by using the averaging function of a fast Fourier transform to increase the reliability of the results.

In the case of rocket pumps using cryogenic fluids, a method to estimate the pump inlet cavitation compliance by the pump inlet reasonant frequency is also often used instead of determining the compliance by measuring dynamic flow rate and pressure. The method uses the following simplified relation between the pump inlet resonant frequency, f_{cr}, and the pump inlet cavitation compliance, C_b.

$$f_{\rm cr} = \frac{1}{2\pi}\sqrt{\frac{1}{L_i C_b}}$$

where L_i is the pump inlet line inertance. In this study, the pump inlet cavitation compliance was also estimated using this method for the experiments without a pump-inlet cryogenic accumulator.

Test Facility

Experiments were conducted using the turbopump test facility shown in Fig. 1 with liquid nitrogen (LN_2) as the pump fluid. Periodic oscillations were generated by a slit type perturbing valve which was installed in the delivery side of the pump. The perturbing valve was comprised of a stationary slit and servo controlled moving slit. The pump was driven by a 450-kW direct current motor/dynamometer, the rotating speed of which could be held at arbitrary values automatically. The moment of inertia of the rotor was so great that fluctuation of the rotating speed could hardly be measured even when flow fluctuations were imposed on the pump. The mean flow rate of the pump was measured by a turbine type flow meter installed in the delivery side of the pump. Dynamic flow rate was measured at the suction side of the pump by an ultrasonic flowmeter having very high response characteristics. The performance of the ultrasonic flowmeter in measuring the dynamic flow rate was confirmed using a piston type dynamic calibration facility.[12] Static flow rate calibration was done by comparing the output of the ultrasonic flowmeter with the output of the calibrated turbine flowmeter in every experiment. Dynamic pressure measurements were carried out using flush mounted quartz-type pressure sensors and strain gage type pressure sensors. An example of flow rate and pressure test data is shown in Fig. 2.

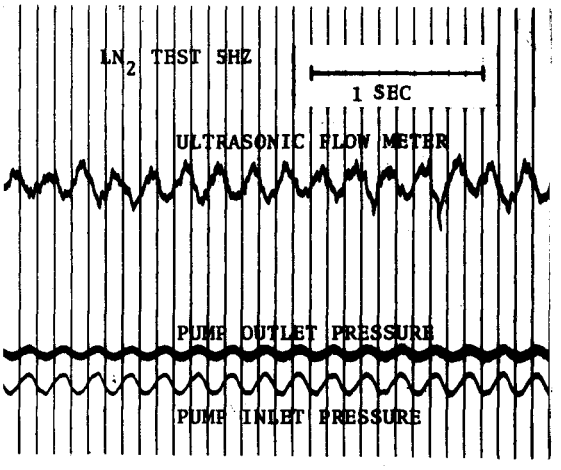

Fig. 2 Example of analog data.

Table 1 Major design characteristics of liquid oxygen turbopump

Speed, rpm	16500
Horsepower, ps	174
Pump type	Single-stage centrifugal pump with an inducer
Pump flow rate, ℓ/s	17.2
Pump delivery head, m	452
Pump required NPSH, m	7.5
Pump efficiency, %	65
Turbine type	Single-stage, two-rotor velocity compound impulse
Turbine inlet pressure, ata	5.0
Turbine outlet pressure, ata	2.2
Turbine efficiency, %	33

Table 2 Main design values of pump

	Inducer	Main impeller
Inlet flow coefficient	0.1	0.151
Outlet flow coefficient	0.121	0.1
Head coefficient	0.16	0.48
Inlet blade angle at tip, deg	10.5	14.3
Outlet blade angle at tip, deg	12.75	25.0
Number of blades	3	6
Outlet diameter, mm	65.3	111.2

Test Pump

The pump tested was part of a liquid oxygen turbopump, the main design values of which are shown in Table 1. This pump was made for purposes of a developmental study of the LOX/LH_2 LE-5 engine which is the second-stage propulsion system of the H-1 rocket. The main design values of the pump inducer and main impeller are shown in Table 2. Further information about the pump is presented in Ref. 13.

Test Results and Discussion

Dynamic Characteristics of the Perturbing Valve

An example of dynamic characteristics of the perturbing valve is shown in Fig. 3. The difference in pressure between points upstream and downstream of the valve, and the amplitude of the valve slit periodical displacement, scarcely affect the dynamic characteristics of the valve. The upper vertical axis of the figure shows a gain, which expresses the ratio of the perturbation command signal wave-amplitude and the actual slit periodical-displacement amplitude on a linear scale. The gain at 1 Hz is assigned a value of one as a standard. As shown in the figure, the gain was over one in the frequency range up to 45 Hz, and the valve worked satisfactorily.

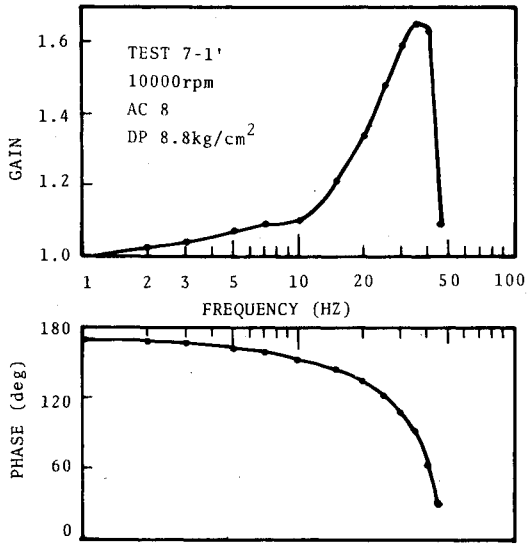

Fig. 3 Dynamic characteristics of perturbing valve.

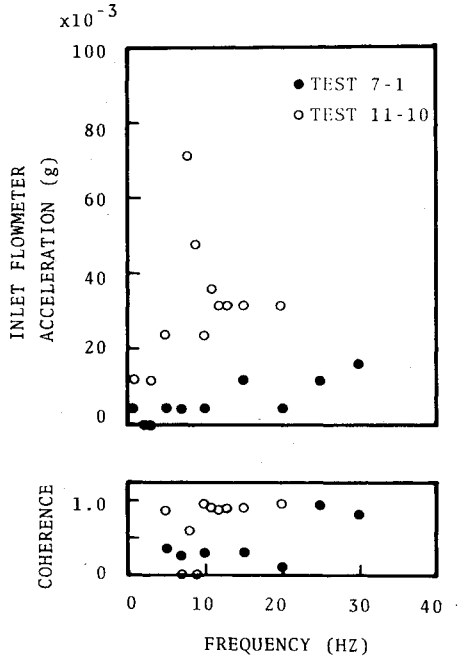

Fig. 4 Acceleration at inlet flow meter.

Flowmeter Acceleration

Vibrations of a flowmeter affect the pump dynamic flow measurement. To examine this effect, acceleration at the flowmeter was measured. Figure 4 shows an example of measured acceleration at the pump inlet flowmeter. Test 7-1 was a high-NPSH experiment at a rotating speed of 10,000 rpm and test 11-10 was a low-NPSH experiment at a speed of 15,000 rpm. In the case of test 11-10, the pump-inlet resonant frequency was 7 Hz. At this frequency the acceleration was larger, though the coherence with the perturbation command signal was small. From these results, it was concluded that the effects of acceleration of the flowmeter on the flow measurement was negligible because the amplitude of the acceleration at every frequency was quite small.

Linearity

Figures 5 and 6 show the results of the experiments in which we examined whether or not linearity existed when the

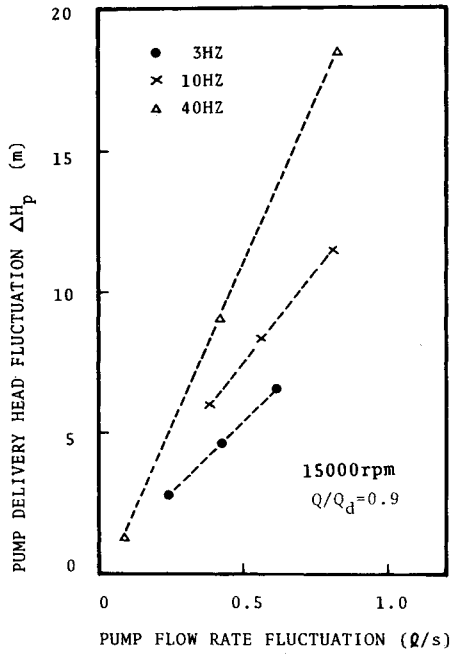

Fig. 5 Amplitude linearity.

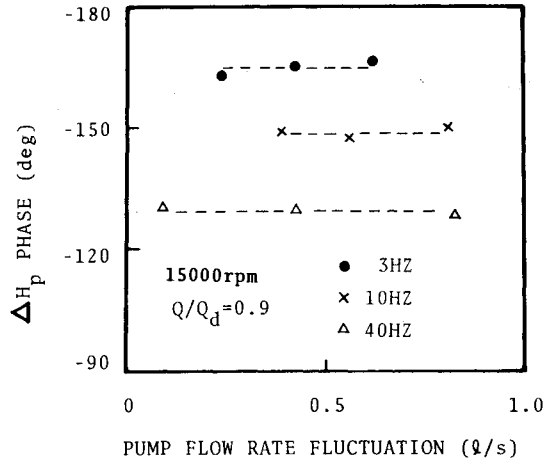

Fig. 6 Phase linearity.

amplitude of the fluctuation was varied under conditions of high NPSH. Figure 5 shows the pump flow rate fluctuation amplitude vs the pump delivery head fluctuation amplitude. The results show that linearity of amplitude existed in most parts of the experiment. The mean flow rate of the experiment shown here was about 14 liters per s. Figure 6 shows the pump flow rate fluctuation amplitude vs the pump delivery head fluctuation phase, relative to the phase of the flow rate fluctuation. The results show that the phase between the flow fluctuation and the pump delivery head fluctuation remained almost constant when the pump flow rate fluctuation was varied and perturbation frequency was kept constant. As the figure shows, with an increase of the frequency the phase tended to approach -90 deg because the component yielded by the pump inertance is larger when the frequency is higher.

The Z_{11} Component

The experimental results regarding the pump transfer matrix Z_{11} component are shown in Figs. 7 and 8. These results were obtained when the rotating speeds were 10,000 and 15,000 rpm. The pump operating conditions of the tests are listed in Table 3. Figure 7 shows the real part of the Z_{11} component. In the case of high pump inlet NPSH, the values are very small. With a reduction of pump inlet NPSH, the real-part value increased.

Given a dynamic system model comprising a cavitation compliance C_b, a mass flow gain factor M_b, a pump dynamic gain factor μ, a resistance R, and an inertance L, the transfer

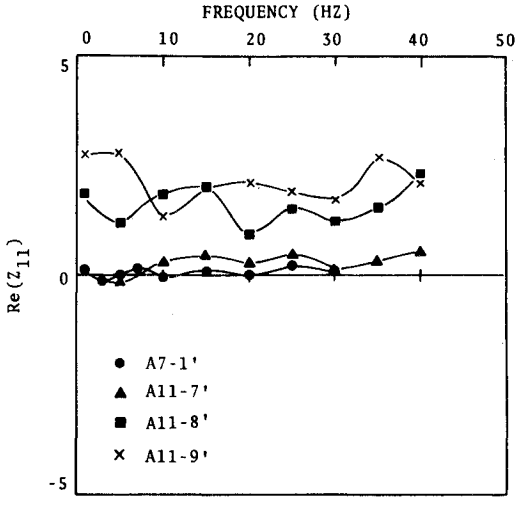

Fig. 7 Real part of Z_{11}.

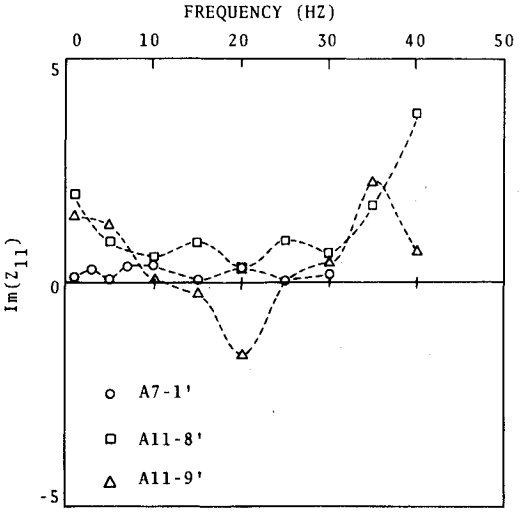

Fig. 8 Imaginary part of Z_{11}.

Table 3 Pump operating conditions (1)

Test no.	Speed, rpm	Flow rate, ℓ/s	Cavitation number
A7-1′	10,000	10.5	0.607
A11-7′	15,000	14.5	0.184
A11-8′	15,000	14.6	0.145
A11-9′	15,000	14.1	0.109
A7-6	5,000	5.1	2.747
A7-5	7,500	7.7	1.122
A7-7	12,500	13.0	0.414
A7-4′	15,000	15.6	0.254
A10-1′	10,000	8.4	0.734
A10-2	10,000	11.5	0.574

matrix components can be expressed as follows:

$$Z_{11} = \mu + j\omega RC_b - \omega^2 LC_b \tag{3}$$

$$Z_{12} = -R + j\omega(RM_b - L) - \omega^2 LM_b \tag{4}$$

$$Z_{21} = -j\omega C_b \tag{5}$$

$$Z_{22} = -j\omega M_b \tag{6}$$

where

$$C_b = -\frac{\partial \bar{V}_c}{\partial \bar{h}_1} \tag{7}$$

$$M_b = -\frac{\partial \bar{V}_c}{\partial \bar{Q}_1} \tag{8}$$

$$\mu = \frac{\partial(\bar{h}_2 - \bar{h}_1)}{\partial \bar{h}_1} \tag{9}$$

From Eq. (3), it is expected that the real part of Z_{11} becomes small when the perturbation frequency is increased under conditions of constant μ, L, and C_b. However, the real-part values of Z_{11} in Fig. 7 do not decrease with an increase of frequency. One possible reason for this is the difference of the pump-inlet pressure-fluctuation amplitude. In the present experiment, with the increase of perturbation frequency, the pump-inlet pressure-fluctuation amplitude became larger. Therefore, the pump operating range of inlet NPSH was thought to extend into a region where the pump dynamic gain μ is greater.

Figure 8 shows the imaginary part of the Z_{11} component. The values of the imaginary part of Z_{11} were small under high NPSH conditions as in the case of the real part of the Z_{11} component. In low-NPSH condition tests, it seemed that the imaginary part of Z_{11} tended to become larger with an increase of frequency in the high frequency region.

The Z_{12} Component

Figure 9 shows a comparison between two results for the Z_{12} component which were determined by different methods. One result was determined by simultaneously solving two equations, $\tilde{h}_{2i} - \tilde{h}_{1i} = Z_{11}\tilde{h}_{1i} + Z_{12}\tilde{Q}_{1i}$ $(i = 1,2)$, derived from two independent sets of data. Another was determined using one set of data assuming the Z_{11} component to be small and negligible, that is $\tilde{h}_2 - \tilde{h}_1 = Z_{12}\tilde{Q}_1$, under high-NPSH conditions. Consequently, Z_{12} was determined by the equation $Z_{12} = (\tilde{h}_2 - \tilde{h}_1)/\tilde{Q}_1$. A centrifugal pump such as the one tested here produces almost all the delivery head by its main impeller. The assumption that the effect of inlet-pressure fluctuation on the pump delivery-head fluctuation is negligible seems therefore to be reasonable, even with relatively low NPSH conditions, at least in the low-frequency region. The difference between the two results determined by different methods seemed to be very small.

The effects of the pump rotating speed on the imaginary and real part of the Z_{12} component are shown in Figs. 10 and 11. The pump operating conditions of the tests are listed in Table 3. The values of each Z_{12} component were determined

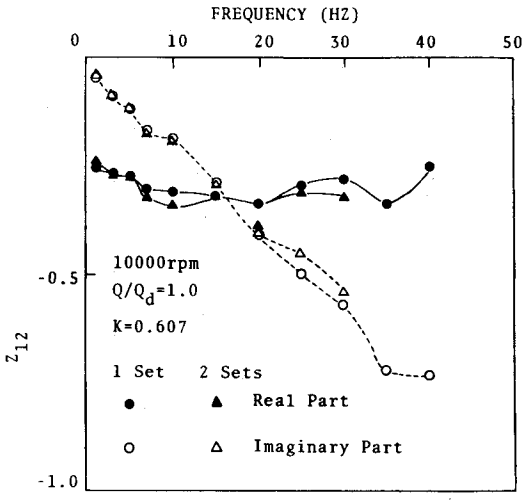

Fig. 9 Comparison of two results.

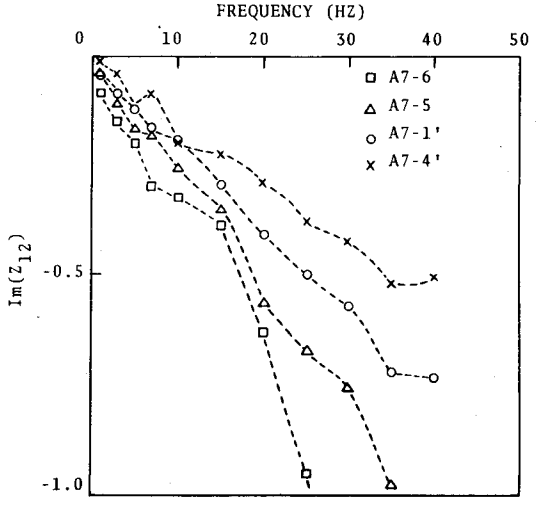

Fig. 10 Effects of rotating speed on imaginary part of Z_{12}.

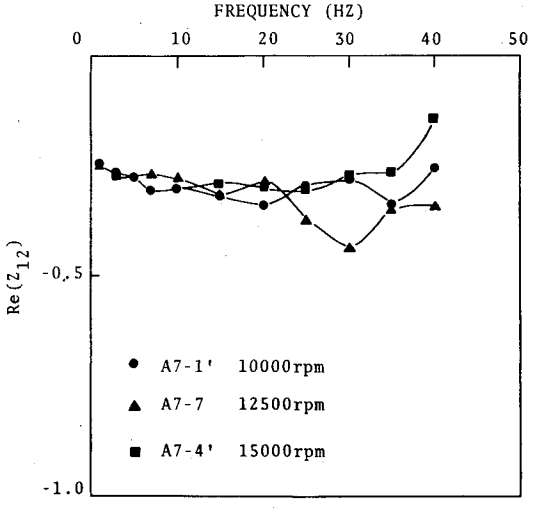

Fig. 11 Effects of rotating speed on real part of Z_{12}.

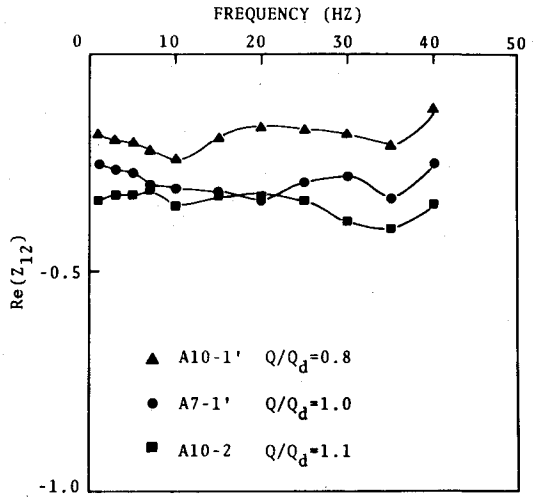

Fig. 12 Effects of mean flow rate on real part of Z_{12}.

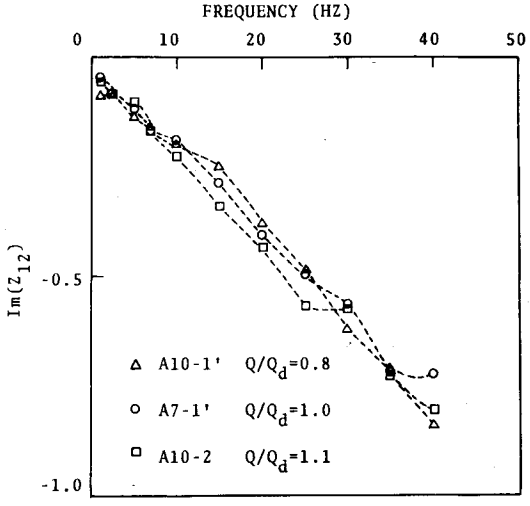

Fig. 13 Effects of mean flow rate on imaginary part of Z_{12}.

by using one set of data. For constant rotating speed, the imaginary-part values of Z_{12} increased almost linearly with frequency. Because the pump head fluctuation was nondimensionalized by dividing it by u_t^2/g, namely twice the main impeller tip velocity head, the slopes of the curves tended to become steep with a decrease of the pump rotational speed. However, the pump inertance values estimated from the imaginary-part slopes and the simplified relation, $Z_{12} = -R - j\omega L$, were almost the same.

Figure 11 shows the effects of the pump rotating speed on the real part of the Z_{12} component. The real-part values of each test having different rotating speeds in the frequency region lower than 20 Hz were nearly the same.

The effects of the pump flow rate on the real and imaginary part of the Z_{12} component are shown in Figs. 12 and 13. The pump operating conditions of the tests are listed in Table 3. With a decrease of the pump flow rate, the real-part values of Z_{12} became smaller. This is considered to be the result of the pump's H-Q curve slope difference. In the case of a centrifugal pump such as the one used in the present study, the H-Q curve is rather flat in the region where the flow rate is less than the design point, so its inclination, $-R$, is small there. The values of the real part of the Z_{12} component in Fig. 12 in the low frequency region were nearly the same as the $-R$ values of the static H-Q curve.

Figure 13 shows the effects of the pump flow rate on the imaginary part of the Z_{12} component. There was not a great difference in the imaginary values of each flow rate over the

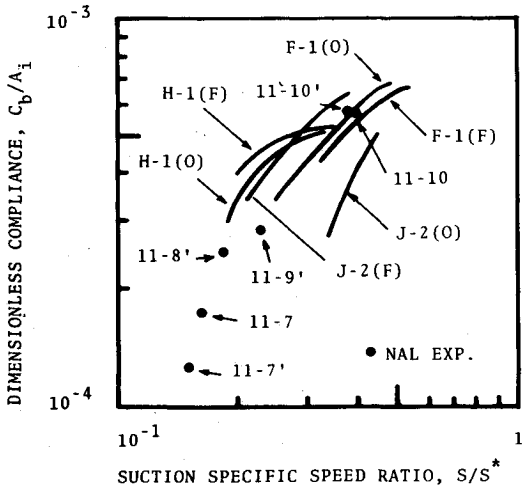

Fig. 14 Cavitation compliance.

Table 4 Pump operating conditions (2)

Test no.	Speed, rpm	Flow rate, ℓ/s	NPSH, m
11-7	15,000	13.7	21.3
11-7′	15,000	13.8	24.1
11-8′	15,000	13.8	18.3
11-9′	15,000	13.7	14.0
11-10	15,000	13.6	6.7
11-10′	15,000	13.8	6.8

whole frequency range, so the effects of the pump mean flow rate are considered to be small.

Pump Inlet Cavitation Compliance

Figure 14 shows the pump inlet cavitation compliance estimated from the test results of the pump inlet resonant frequencies compared with the compliance of the rocket pumps in Ref. 14. Pump operating conditions of the tests conducted here are listed in Table 4. The large dots in the figure signify the results of the experiments in this study. Cavitation compliance in the vertical axis was nondimensionalized by dividing it by the pump inlet cross sectional area, A_i. The horizontal axis shows nondimensionalized suction specific speed which is defined by S/S^*. S denotes suction specific speed and $*$ denotes the value at the cavitation breakdown point. F-1, H-1, and J-2 in the figure are names of rocket engines, and (0) and (F) designate the oxydizer and fuel systems, respectively. As seen in the figure, the test results showed that the nondimensionalized cavitation compliance values of the pump used in the present study fell in the same region as the nondimensionalized cavitation compliance values of the pumps in Ref. 14.

Concluding Remarks

In the present paper experimental results regarding the pump dynamic response of a cryogenic centrifugal pump with an inducer are shown. These are required for POGO analysis of the H-1 rocket. In particular, the two components Z_{11} and Z_{12} of the pump dynamic transfer matrix were investigated by using two sets of independent data obtained under the same mean operating conditions, but having different phase relationships between pressure fluctuations and flow fluctuations. These fluctuations were generated by a slit type perturbing valve. Independent sets of data were obtained by varying the helium gas volume in a vacuum-jacketed cryogenic accumulator which was installed in the pump suction line. The dynamic flow rate was measured by the ultrasonic flow meter in Ref. 12. Using this experimental technique, independent sets of data were obtained successfully, and the Z_{11} and Z_{12} components were determined. The pump inlet cavitation compliance was also estimated with a method using the pump inlet resonant frequency and compared with the values of the rocket pumps in Ref. 14. Detailed results are as follows:

1) Linearity of amplitude existed in most parts of the experiment, and the phase remained almost constant when the fluctuation amplitude was varied under high NPSH conditions.

2) Both the real- and imaginary-part values of the Z_{11} component were very small under high-inlet NPSH conditions. The real-part values of the component increased with the reduction of pump inlet NPSH and remained almost constant with the increase of frequency. The imaginary-part values of the component tended to become larger with the increase of frequency in the high frequency region.

3) The Z_{12} component was determined by two different methods in order to examine the reasonableness of the assumption that Z_{11} is negligible. The difference between the two results was very small, and the assumption seemed to be reasonable. The imaginary-part values of the Z_{12} component increased almost linearly with frequency, and pump inertance values estimated from the different rotational speed data were almost the same. The effects of the pump mean flow rate on the imaginary part of the Z_{12} were small. The test results showed that dependency of the Z_{12} component on frequency was small. Therefore it was concluded that a quasistatic treatment of the Z_{12} component is applicable to a centrifugal pump, such as the one used in this study, up to relatively high frequency regions.

4) The cavitation compliance values of the present pump estimated from the pump inlet resonant frequency fell in the same region as the cavitation compliance values of the rocket pumps in Ref. 14.

References

[1]Rubin, S., "Longitudinal Instability of Liquid Rockets due to Propulsion Feedback (POGO)," *Journal of Spacecraft and Rockets*, Vol. 3, Aug. 1966, pp. 1188-1195.

[2]"Prevention of Coupled Structure-Propulsion Instability (POGO)," NASA SP-8055, Oct. 1970.

[3]Acosta, A.J., "An Experimental Study of Cavitating Inducers," *Second Symposium on Naval Hydrodynamics*, Aug. 1958, pp. 533-557.

[4]Brennen, C. and Acosta, A.J., "Theoretical Quasi-Static Analysis of Cavitation Compliance in Turbopumps," *Journal of Spacecraft and Rockets*, Vol. 10, March 1973, pp. 175-180.

[5]Young, W.E., et al., "Study of Cavitating Inducer Instabilities—Final Report," NASA CR-123939, 1973.

[6]Brennen, C. and Acosta, A.J., "The Dynamic Transfer Function for a Cavitating Inducer," *ASME Journal of Fluids Engineering*, Vol. 98, June 1976, pp. 182-191.

[7]Ng, S.L. and Brennen, C., "Experiments on Dynamic Behavior of Cavitating Pumps," *ASME Journal of Fluids Engineering*, Vol. 100, June 1978, pp. 166-176.

[8]Brennen, C., et al., "Scale Effects in the Dynamic Transfer Functions for Cavitating Inducers," *ASME Journal of Fluids Engineering*, Vol. 104, Dec. 1982, pp. 428-433.

[9]Ohashi, H., "A Study of Turbopump Dynamic Characteristics," *Transactions of the Japan Society of Mechanical Engineers*, Vol. 33, Nov. 1967, pp. 1789-1799.

[10]Anderson, D.A., Blade, R.J., and Steven, W., "Response of a Radial-Blades Centrifugal Pump to Sinusoidal Disturbances for Non-Cavitating Flow," NASA TN D-6556, 1971.

[11]Ghahremani, F.G. and Rubin, S., "Empirical Evaluation of Pump Inlet Compliance—Final Report," ATR-73(7257)-I, The Aerospace Corporation, El Segundo, Calif., 1972.

[12]"Calibration of Ultrasonic Flowmeters," ONERA Activities, 1975, pp. 88-89.

[13]Kamijo, K., et al., "Development of Liquid Oxygen and Hydrogen Turbopumps for the LE-5 Rocket Engine," *Journal of Spacecraft and Rockets*, Vol. 19, May-June 1982, pp. 226-231.

[14]Rubin, S., Wanger, R.G., and Payne, J.G., "POGO Suppression on Space Shuttle Early Studies," NASA CR-2210, 1973.